International Journal of Network Dynamics and Intelligence Scilight

Article

A Novel CEEMD-Based Multichannel Denoising Autoencoder for Noise Attenuation of Surface Microseismic Data

Chuang Guan [1,2], Lujia Zheng [1,2], and Chuang Wang [1,2,*]

[1] Key Laboratory of Continental Shale Hydrocarbon Accumulation and Efficient Development, Ministry of Education, Northeast Petroleum University, Daqing 163318, China
[2] Heilongjiang Provincial Key Laboratory of Networking and Intelligent Control, Northeast Petroleum University, Daqing 163318, China
[*] Correspondence: wangchuang64@126.com

Received: 30 March 2025
Accepted: 30 September 2025
Published: 16 December 2025

Abstract: Surface microseismic data (SMD) are usually presented as weak signals affected by strong interference. In this paper, with the purpose of obtaining available SMD, a deep learning framework combining with the complete ensemble empirical mode decomposition (CEEMD) and the multichannel denoising autoencoder (MDAE) is established to strengthen weak signals and suppress strong interference. First of all, a sort of EMD algorithm referred to as CEEMD is employed to decompose each trace of the SMD into the intrinsic mode functions (IMFs) so as to reduce the interference of random noise. Then, an MDAE algorithm is put forward to extract the effective and robust features of the IMFs, where a novel loss function without any label information is designed to achieve unsupervised noise attenuation in the real-world scenario. After that, the decomposed IMFs are reconstructed from high frequency to low frequency by using the extracted features such that the high-frequency part of the microseismic signals is retained effectively. Finally, the proposed CEEMD-MDAE model is applied to the noise attenuation in both synthetic and real-world SMD datasets. Experimental results demonstrate that the CEEMD-MDAE algorithm significantly improves the signal-to-noise ratio and outperforms some existing popular denoising algorithms.

Keywords: noise attenuation; multichannel denoising autoencoder; unsupervised learning strategy; complete ensemble empirical mode decomposition; surface microseismic data

1. Introduction

Over the past decades, microseismic monitoring technology has played an increasingly prominent role in the exploration and exploitation of unconventional oil and gas resources. Generally, microseismic monitoring patterns can be roughly grouped into two categories, including surface monitoring and borehole monitoring. Compared with the borehole monitoring pattern, the surface monitoring pattern has the distinctive characteristics of flexibility, low investment and large coverage [1–5]. Nevertheless, during the exploitation of unconventional oil and gas, the received signals of the surface monitoring pattern is greatly affected by surrounding environment noise. The strong interference contained in microseismic data is not conducive to carrying out follow-up works such as microseismic phase identification, first break extraction and fracture interpretation. To alleviate these problems, it is necessary to attenuate the noise coupled in the microseismic signals and separate the effective signals from the noisy data accurately.

Till now, many efforts have been made to explore the noise attenuation methods with the aim to increase the fidelity of the signals, see [6–12]. According to the properties of the microseismic signals, the noise attenuation methods can be divided into the following two categories: 1) model denoising method; and 2) data-driven denoising method. As shown in Figure 1, among these methods, the empirical mode decomposition (EMD) algorithm has been extensively applied into the signals denoising owing to its characteristics of posteriority and adaptive decomposition, see [13–16].

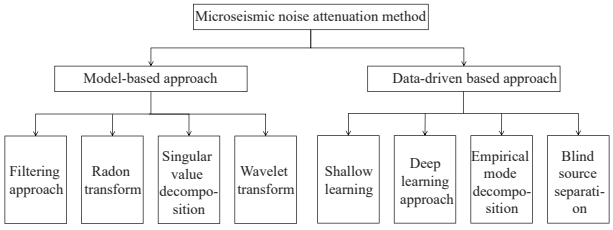

Figure 1. The diagram of the different microseismic noise attenuation methods.

Despite the powerful decomposition and denoising ability, the EMD method still suffers from the problem of mode mixing, and thus a complete ensemble empirical mode decomposition (CEEMD) algorithm has been proposed, where positive and negative white noise are added to solve the problem of mode mixing. For example, a CEEMD method with wavelet threshold denoising has been proposed in [17] to preserve the effective information of high-frequency signals. Very recently, a joint denoising method of wavelet threshold and CEEMD based on compression perception has been developed in [18] to preserve weakly effective signals. In addition, in order to realize microseismic noise attenuation, a compressed sensing method based on improved CEEMD has been investigated in [19] to enhance the signal fidelities and retain effective signal amplitudes. Unfortunately, the CEEMD method attenuates the noise by discarding the high-frequency component of the original signals, which results in the loss of effective signals [20]. Therefore, the tricky part of noise attenuation is how to improve the denoising capability while retaining the effective signals in the whole frequency range [21].

In recent years, deep learning technique has attracted widespread interest due to its powerful capabilities in feature extraction and representation [22–34]. For instance, a convolutional neural network (CNN) with residual dense blocks has been proposed in [27] to fit the seismic signals with high signal-to-noise ratio, which has achieved superior performance in the seismic data processing. Nevertheless, the CNN-based denoising model cannot preserve the textural features of seismic data. For this reason, denoising autoencoder (DAE) has been extensively researched in the field of noise attenuation with its advantages of feature extraction and generalization, and considerable results have been reported [35–40]. For instance, an improved DAE network has been presented in [40], which has the capacity to extract effective features of the data in an unsupervised way. Moreover, a convolutional autoencoder-based noise attenuation method has been proposed in [35] to address the seismic texture structure distortion. Nonetheless, it still causes the loss of the representative signals when the effective signals are separated from the data. Note that there are few in-depth studies on the application of DAE network in the field of noise attenuation, which inspires to develop data-driven methods for microseismic noise suppression.

In this paper, a novel noise attenuation method is proposed to separate the microseismic signals from the noisy data accurately and effectively. The main contributions of this paper are outlined as follows.

1) A novel noise attenuation method is proposed, where the IMFs obtained from the CEEMD are used as the input of the multichannel network, and then the MDAE algorithm is put forward to extract the features and the reconstruct signals for noise suppression.

2) A novel loss function is proposed for denoising microseismic data in an unsupervised manner, which is capable of avoiding the loss of the effective signals of the microseismic data.

3) The proposed CEEMD-MDAE noise attenuation method is evaluated on synthetic and real-world datasets. Experimental results demonstrate that the proposed method exhibits better performance than some classical algorithms.

The remaining part of this paper is organized as follows. The preliminaries of the CEEMD and deep autoencoder are introduced in Section II. A novel CEEMD-MDAE model is proposed to attenuate noise in Section III. The process and results of the experiments are presented in Section IV. Finally, conclusions and prospects are presented in Section V.

2. Preliminaries

2.1. Complete Ensemble Empirical Mode Decomposition

As an adaptive time-frequency signal processing method, EMD has been proposed by Huang and Shen in 1998 to deal with the analysis problem of nonlinear and non-stationary data [15]. Owing to the advantages of posteriority and stability, the EMD has been applied to deal with seismic data in the field of geological exploration. Nevertheless, the discontinuity of signals may cause the mode aliasing in the decomposition process of the EMD, thereby losing partial mode components. To tackle this issue, the white noise subjected to normal distribution has been introduced

into the signals by the ensemble empirical mode decomposition (EEMD) such that the new signal satisfies the continuity and is automatically distributed with appropriate scale [41]. Although this method can address the problem of mode aliasing to some extent, the additional noise can not be ignored after reconstruction.

In this case, as a variant of the EEMD, the CEEMD has been proposed [20] to handle the additional noise. In the CEEMD method, the original signals with positive and negative white noise are decomposed simultaneously by the EMD, thereby cancelling the additional noise in the signals. The CEEMD retains the benefits of both the EMD and EEMD, and thus reduce the redundant noise effectively. The decomposition steps of the CEEMD are displayed as follows.

1) Introducing the positive and negative white noise into original signals, the new signals can be expressed by

$$\begin{cases} E_{i1}(t) = x(t) + n_i(t) \\ E_{i2}(t) = x(t) - n_i(t) \end{cases} \tag{1}$$

where $x(t)$ is the original signal, and $n_i(t)$ represents the Gaussian white noise. $E_{i1}(t)$ and $E_{i2}(t)$ are the new signals.

2) The EMD is performed for obtaining signals $E_{i1}(t)$ and $E_{i2}(t)$, respectively.

Step 1. Calculating all extremum points of $E_{i1}(t)$ and using cubic spline interpolation to fit the upper and lower envelope of $E_{i1}(t)$, the signal margin is described as follows:

$$h_1(t) = E_{i1}(t) - m_1(t) \tag{2}$$

where $m_1(t)$ is the mean value of upper and lower envelope, and $h_1(t)$ represents the signal margin.

Step 2. Repeat step 1 for the remaining component $h_1(t)$ until it satisfies the following two conditions of the EMD: a) the number of extremum and zeros points must be equal or at most only one different over the whole signal degree; and b) the average of the upper and lower envelope is zero at any time.

Step 3. After obtaining the highest frequency component, which is called $IMF_1(t)$, the residual signal $r_1(t)$ is calculated as follows:

$$r_1(t) = E_{i1}(t) - IMF_1(t) \tag{3}$$

Step 4. Repeat steps 1-3 to obtain a series of mode components:

$$y_{i1}(t) = \sum_{k=1}^{K} IMF_k(t) + R(t) \tag{4}$$

where K is the number of intrinsic mode functions, and $R(t)$ denotes the residual signals.

Step 5. Execute steps 1-4 to acquire a set of signal components and signal margins.

3) The final intrinsic mode functions and residual signals can be obtained by averaging the signal components gained by decomposing $E_{i1}(t)$ and $E_{i2}(t)$, respectively.

2.2. Denoising Autoencoder

As a classical unsupervised learning method, the autoencoder has been proposed in 1987 consisting of encoder and decoder [42]. In the encoding process, the effective features are extracted from input data in the hidden layer. In the decoding process, the extracted robust features are reconstructed as the output data [43]. As a variant of the autoencoder, DAE attempts to encode the input in some degree that can eliminate the effects of a random corruption process, which exhibits significant advantages of reducing the dependency among input dimensions and improving the feature extraction capability. The schematic diagram of a DAE is depicted in Figure 2.

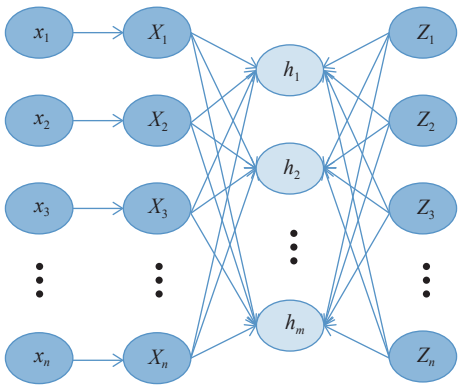

Figure 2. The structure of the DAE network.

As shown in Figure 2, a DAE consists of the noise-adding layer, the encoding layer and the decoding layer. $x = (x_1, x_2, \cdots, x_n)$ is the clean data (i.e., the input of the DAE network), $X = (X_1, X_2, \cdots, X_n)$ denotes the data with noise, $h = (h_1, h_2, \cdots, h_m)$ represents the hidden state, and $z = (z_1, z_2, \cdots, z_n)$ is the output of the DAE network.

In the encoding stage, h is obtained by a nonlinear mapping of X to the hidden layer through the function f, and the mapping relation is given as follows:

$$h = f(X) = s(w_1 X + b_1) \tag{5}$$

where w_1 is the full connection weight matrix between the input layer and the hidden layer, and b_1 represents the bias vector of the input layer. $s(\cdot)$ uses Relu as the activation function.

In the decoding stage, z is gained by h mapped to the output layer through the decoding function g, which is described as follows:

$$z = g(h) = s(w_2 h + b_2) \tag{6}$$

where w_2 denotes the weight matrix between the hidden layer and the output layer, and b_2 represents the bias vector of the hidden layer. Note that z has the same number of the sampling points as x.

Define a new variable $\theta = \{w_1, w_2, b_1, b_2\}$ (i.e., the collection of all parameters in denoising network), and the reconstruction error is minimized by adjusting θ. The error between x and z is regarded as reconstruction error, which can be calculated by

$$J_{\mathrm{DAEcost}}(\theta) = \frac{1}{n}\sum_{i=1}^{n} \|z_i - x_i\|_2^2 \tag{7}$$

where n is the number of samples, whereas x_i and z_i represent the input data and output data of the DAE network.

3. The Ceemd-mdae Method

3.1. Synthetic Microseismic Data

In the microseismic data processing, the most basic requirements are high signal-to-noise ratio and high fidelity. The ideal noise suppression effect is to completely separate the effective signals from the noise. In practical terms, the clean field microseismic data are unknown or even the effective signals are completely submerged by noise, making it difficult to effectively remove the noise from the microseismic data. As such, this paper proposes the CEEMD-MDAE to solve the above problem, where the synthetic microseismic data are utilized to train the denoising model firstly, and then the trained model is exploited to suppress noise from the field data. Note that the synthesis of the microseismic data is essential because the prior clean signals and noise are not available from the field data.

The Ricker wavelet has the characteristics of short duration and fast convergence, which is similar to the surface microseismic data. Hence, it is suitable to be applied to microseismic data simulation, and the relation of Ricker wavelet $g(t)$ can be obtained as follows:

$$\begin{cases} g(t) = [1 - 2(\pi f t)^2] \times e^{[-(\pi f t)^2)]} \\ t = k\Delta t \end{cases} \tag{8}$$

where f is the main frequency of wavelet, k represents the sampling sequence, and Δt is the sampling interval.

The synthesis of microseismic data is a one-dimensional forward process, which is obtained via the convolution of reflection coefficient and microseismic wavelet. The specific expression is as follows:

$$S(t) = R(t) * L(t) \tag{9}$$

where $S(t)$ denotes the synthetic microseismic data, $R(t)$ and $L(t)$ are the reflection coefficient and microseismic wavelet, respectively. The reflection coefficient can be calculated as follows:

$$R_i = \frac{\rho_{i+1} v_{i+1} - \rho_i v_i}{\rho_{i+1} v_{i+1} + \rho_i v_i} \tag{10}$$

where R_i represents the reflection coefficient of the interface between the current layer and the next layer, ρ_i and v_i are the density and velocity of the current layer. ρ_{i+1} and v_{i+1} are the density and the velocity of the next layer, respectively.

3.2. The Process of the CEEMD-MDAE Method

The proposed method utilizes the Ricker wavelet to synthesize the clean microseismic data and adds the

Gaussian white noise for obtaining the noisy data, then uses the noisy data to carry on the simulation of microseismic denoising. The procedure of this method are as follows. Firstly, for the noisy microseismic data, each trace of raw data is decomposed into five intrinsic mode components. It is worth noting that the mode function components have the same trace sets and sampling points as the original data, which are distributed from high to low frequency. Secondly, all the modes obtained from the decomposition are fed into the MDAE network, with each mode component corresponding to one channel of the multichannel denoising network. Thirdly, in the MDAE network, the effective features of microseismic data are extracted via dimensionality reduction in the encoding layer. Then, the clean data are reconstructed in the decoding layer by using the extracted effective features. Finally, The multichannel denoising network is reconstructed to obtain the final network output. Note that the network structure of the encoding layer and decoding layer are symmetric. In this way, the MDAE network achieves to remove redundant noise and retains weak effective signals. The process of the proposed method is shown in Algorithm 1.

Algorithm 1. The process of the proposed algorithm

Step 1.	Synthetic data Microseismic data are synthesized by convolution of Ricker wavelet and reflection coefficient.
Step 2.	Model decomposition The synthesized microseismic data are divided into five intrinsic modes.
Step 3.	Feature extraction The MDAE network is adopted to extract features automatically.
Step 4.	Feature reconstruction The extracted features are reconstructed and the noise suppression is completed simultaneously.
Step 5.	Stop.

In the field data, clean microseismic data are difficult to acquire, which results in the clean data being unlabelled. Therefore, microseismic data denoising needs to be carried out in an unsupervised way. In order to better suppress the microseismic data noise, a new loss function is proposed for microseismic data denoising in an unsupervised manner, which is shown as

$$J_{cost} = \frac{1}{n}\sum_{i=1}^{n}\frac{1}{2}\|SD_i - S_i\|_2^2 + \frac{\sum_{i=1}^{n}(SD_i - \overline{SD_i})(SN_i - \overline{SN_i})}{\sqrt{\sum_{i=1}^{n}(SD_i - \overline{SD_i})^2 \sum_{i=1}^{n}(SN_i - \overline{SN_i})^2}} \tag{11}$$

where SD_i and SN_i are denoised data and removed noise obtained by proposed method, and $\overline{SD_i}$ and $\overline{SN_i}$ are the average value of denoised data and removed noise, respectively. S_i and n represent the clean microseismic data and the number of samples. Note that (11) can be used when noise suppression is performed on the synthetic data. Nevertheless, the field microseismic data are generally noisy and there are no clean data, so the reconstruction error of the denoised data and clean data can not be used to define the loss function. Therefore, the second term of (11) is used as the loss function for the field microseismic data.

In order to minimize the value of the loss function, the weight and deviation of each layer in the MDAE network are adjusted, and the updated values are taken as the parameters of each layer in the denoising network. In this way, the MDAE network has better denoising and generalization performance. Then, fine-tune the trained network to suppress the noise of the field surface microseismic data, and further achieve the goal of noise attenuation in an unsupervised manner.

3.3. Framework of the CEEMD-MDAE Algorithm

The framework of the CEEMD-MDAE algorithm is shown in Figure 3.

4. Experimental Simulation and Discussion of the Proposed Model

In order to comprehensively evaluate the proposed method, two examples of synthetic data and field surface microseismic data are used to compare the CEEMD-MDAE with several classical denoising methods such as the CEEMD, DAE, GAN and CEEMD-SVD method [44–47]. Among them, the synthetic data contain different conditions such as parallel, crossed and bended events with different signal-to-noise ratios. In addition, the field data also include nonlinear and crossing events. To accurately measure the performance of our proposed algorithm on removing noise and retaining effective signals, the signal-to-noise ratio (SNR) and mean square error (MSE) are regarded as evaluation criteria, which are defined as follows:

$$\mathrm{SNR} = 10\log\frac{\|S\|^2}{\|S - S_N\|^2} \tag{12}$$

$$\mathrm{MSE} = \frac{1}{M}\|S - S_N\|_2^2 \tag{13}$$

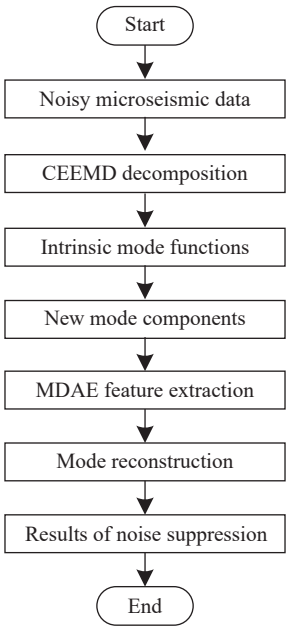

Figure 3. The flowchart of the CEEMD-MDAE framework.

where S and S_N are the clean data and the noisy data, and M represents the length of the data.

4.1. Synthetic Examples

In this subsection, the Ricker wavelet generates the clean microseismic data with sampling interval of 1 ms and dominant frequency of 45 Hz, containing three linear events and one nonlinear event, as shown in Figure 4. Then, Gaussian noise is added to the clean microseismic data, as shown in Figure 5(a), the SNR of the signals after adding noise is −5.8 dB. In addition, the 10 th trace of the noisy data is taken for mode decomposition, as shown in Figure 5(b), where the first subfigure shows the single channel noisy microseismic data and the remaining five subfigures represent the intrinsic mode components decomposed from high to low frequency. The CEEMD, CEEMD-SVD and DAE are adopted to compare with the proposed method in terms of suppressing noise, and the results are shown in Figure 6. The SNR of the signals processed by the CEEMD, CEEMD-SVD, DAE and the proposed method are 3.86 dB, 4.10 dB, 6.02 dB and 8.70 dB, respectively, which shows that the CEEMD-MDAE has a better ability to separate noise from the microseismic data for such nonlinear events. Compared with the proposed method, the CEEMD and CEEMD-SVD still retain more random noise, and the fidelity of the effective signals is not very high. In addition, the DAE has a better noise suppression effect than those in Figures 6(a) and 6(b), but there are still some effective signal losses.

The MSE of the signals processed by the CEEMD, CEEMD-SVD, DAE and the proposed method are 0.0054, 0.0064, 0.0015 and 0.000025, respectively. Although the CEEMD-SVD is better than CEEMD in noise suppression, MSE is slightly larger. The DAE is better than the first two methods in terms of MSE and SNR of microseismic data, while the proposed method is superior to DAE algorithm in these two evaluation indicators. In addition, the separated noise signals are shown in Figure 7. It can be seen from Figure 7(c) that the noise section contains effective signal residues, which indicates that the DAE can adversely affect the subsequent processing of microseismic data. To sum up, the CEEMD-MDAE method not only can remove the noise well, but also can achieve the retention of more effective weak microseismic signals.

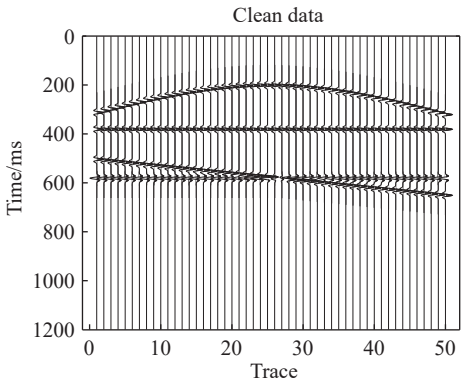

Figure 4. The generated clean microseismic data.

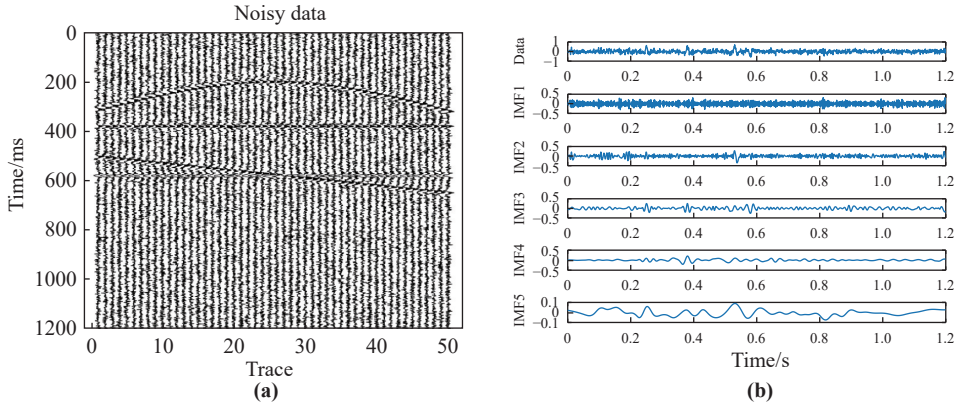

Figure 5. (a) The generated noisy data. (b) The IMFs of the data.

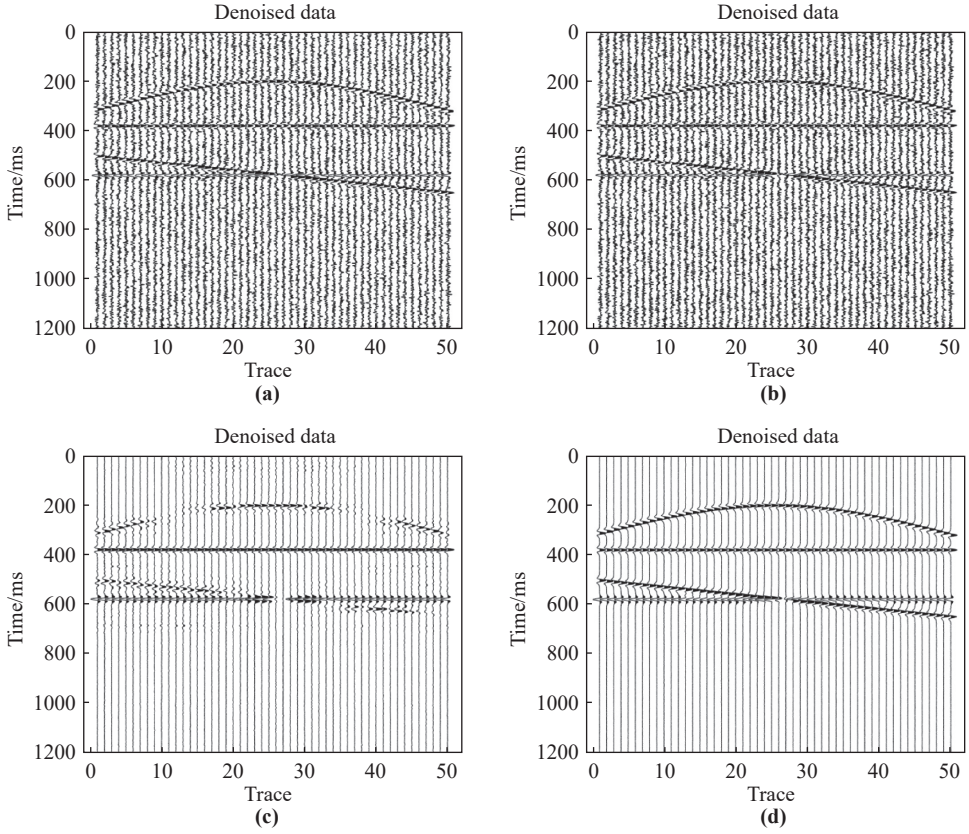

Figure 6. (a) The CEEMD denoised section. (b) The CEEMD-SVD denoised section. (c) The DAE denoised section. (d) The CEEMD-MDAE denoised section.

The synthetic data of the second example are shown in Figure 8(a), which contains clean microseismic data with parallel and cross events. As shown in Figure 8(b), random noise is added to clean microseismic data. The proposed method is compared with several benchmark denoising methods and the results are shown in Figure 9. It is clear that SNR of raw data is −5.5 dB, while the SNR of the signals processed by the CEEMD and CEEMD-SVD are raised to 3.95 dB and 4.15 dB, respectively. Note that the DAE can improve the SNR to 7.78 dB, but is still lower than 9.29 dB of the proposed method. In addition, it can be seen from Figures 10(c) and 10(d) that the DAE method has obvious linear event residues, while CEEMD-MDAE method has relatively few effective signal residues in the noise part after denoising. Although the CEEMD and CEEMD-SVD retain more effective microseismic information than the DAE after denoising, the performance of the noise suppression is not as good as that of the proposed method. In terms of MSE, the DAE denoising method has the lowest value of 0.000093 and the CEEMD method has the highest value of 0.0095, whereas the MSE of the proposed method is 0.00074. Moreover, the SNR and MSE comparison for the four methods of two examples are shown in Table 1 and Table 2. From Tables 1-2 and the obtained simulation results of four methods, it is clear that the proposed method has better noise suppression

effect and greater ability to retain weak effective signals. Although MSE in the second example is slightly higher, the performance of the proposed method is generally superior to other methods.

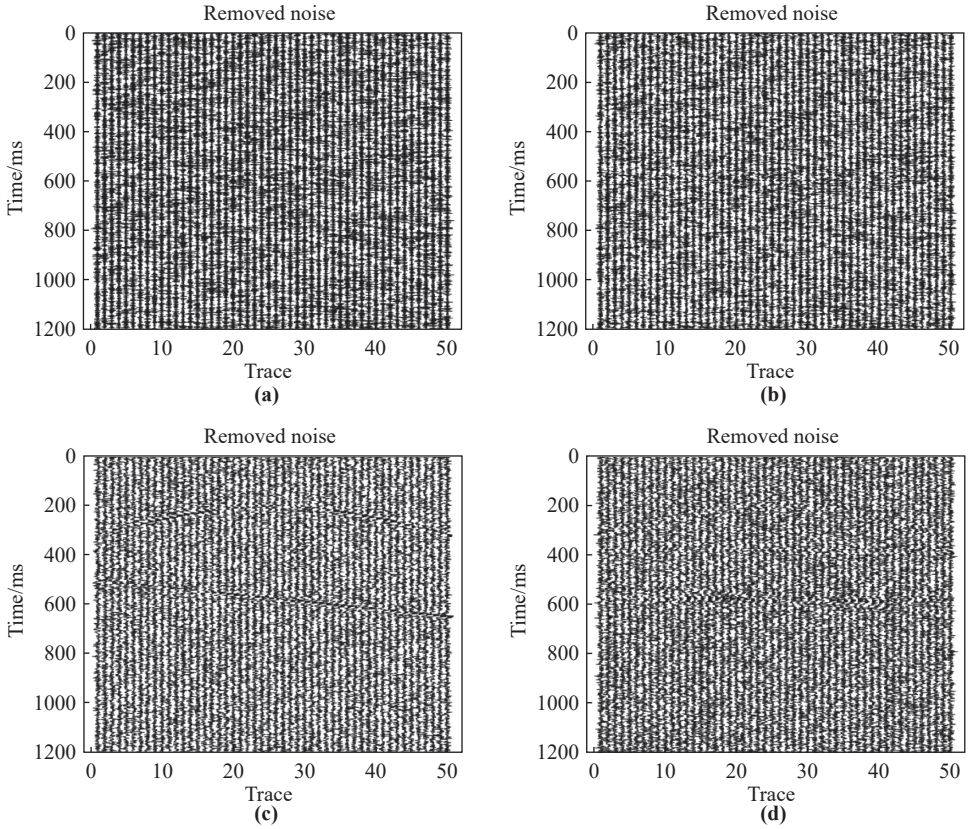

Figure 7. (a) The CEEMD noise section. (b) The CEEMD-SVD noise section. (c) The DAE noise section. (d) Noise section using the proposed CEEMD-MDAE.

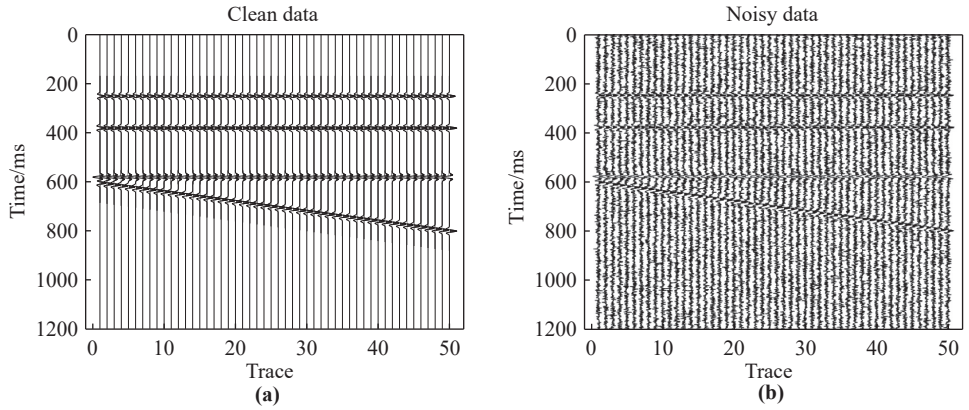

Figure 8. (a) Clean data in example 2. (b) Noisy data in example 2.

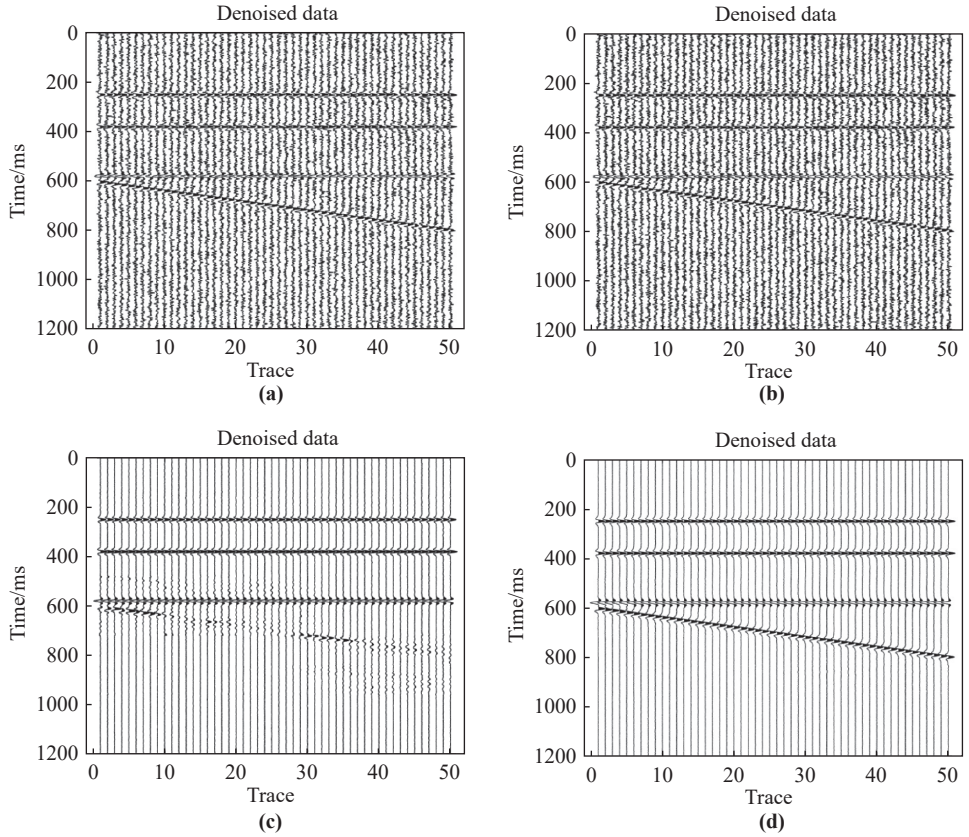

Figure 9. (a) The CEEMD denoised section. (b) The CEEMD-SVD denoised section. (c) The DAE denoised section. (d) The CEEMD-MDAE denoised section.

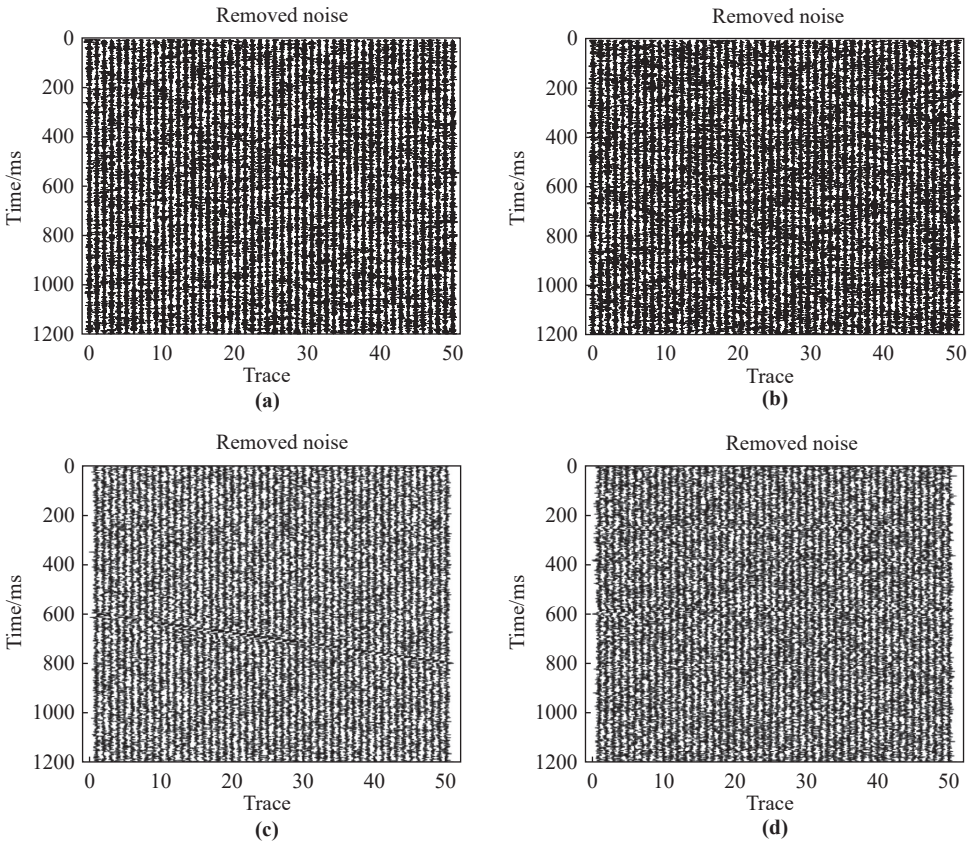

Figure 10. (a) The CEEMD noise section. (b) The CEEMD-SVD noise section. (c) The DAE noise section. (d) Noise section using the proposed CEEMD-MDAE.

Table 1 The SNR of the Signals Processed via Four Methods

Method	Example 1 SNR(dB)	Example 2 SNR(dB)
Synthetic data	−5.8	−5.5
CEEMD	3.86	3.95
CEEMD-SVD	4.10	4.15
DAE	6.02	7.78
Proposed method	8.70	9.29

Table 2 The MSE of the Signals Processed via Four Methods

Method	Example 1 SNR(dB)	Example 2 SNR(dB)
CEEMD	0.0054	0.0095
CEEMD-SVD	0.0064	0.0017
DAE	0.0015	0.000093
Proposed method	0.000025	0.00074

4.2. Field Data Example

In this section, the denoising network obtained by training synthetic data is fine-tuned via field surface microseismic data. Nevertheless, the clean data are hard to obtain in the field microseismic data and the SNR can no longer be used to measure the effectiveness of denoising. Therefore, the similarity between the denoised data and the removed noise is employed as the measurement index.

Figure 11 shows the field data, which includes discontinuous events, nonlinear events and partial loss of effective signals. Although the SNR can not be used to measure the effect of denoising, some conclusions can still be drawn from the perspective of the microseismic event since it has important impact on the subsequent interpretation of denoising. The denoising results of the CEEMD, CEEMD-SVD, DAE and the proposed method are shown in Figure 12. It can be seen that these methods have certain noise suppression effect. Among them, the CEEMD contains a large number of random noise signals after denoising, so it has the worst effect in noise reduction. The CEEMD-SVD has a certain improvement in noise suppression, but the fidelity after denoising is too low, which results in unclear microseismic event information. Compared with the first two methods, the DAE has better performance in noise suppression. Figure 13 shows the section of noise removed by the four methods. In Figure 13(c), it can be seen that part of the effective signals processed by the DAE is also regarded as noise, which leads to that the noise section still contains structural information. Meanwhile, Figures 12(d) and 13(d) illustrate that the proposed method is superior to other methods in noise suppression and effective signal retention. In addition, Figure 14 shows the similarity of the removed noise and the denoised data by four methods. The lower the similarity is, the better the denoising effect is. As can be seen from Figure 14 that the CEEMD and CEEMD-SVD are not as effective as the DAE and CEEMD-MDAE methods in noise suppression. It can also be seen from Figure 14(c) that the noise section removed by the DAE contains certain effective signals, which results in a high local similarity between the noise and the effective signals. Compared with other methods, the similarity between the noise removed by the proposed method and the denoised section is lower, which also proves the superiority of the proposed method in noise attenuation and effective signal retention, thereby making the data interpretation more convenient after denoising.

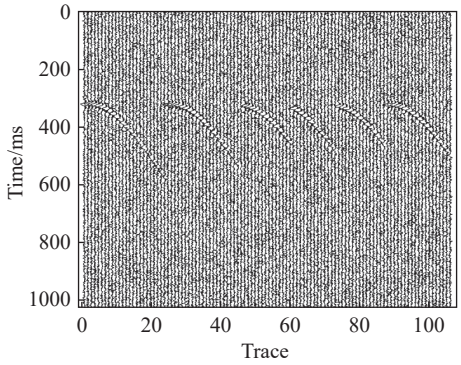

Figure 11. Field data.

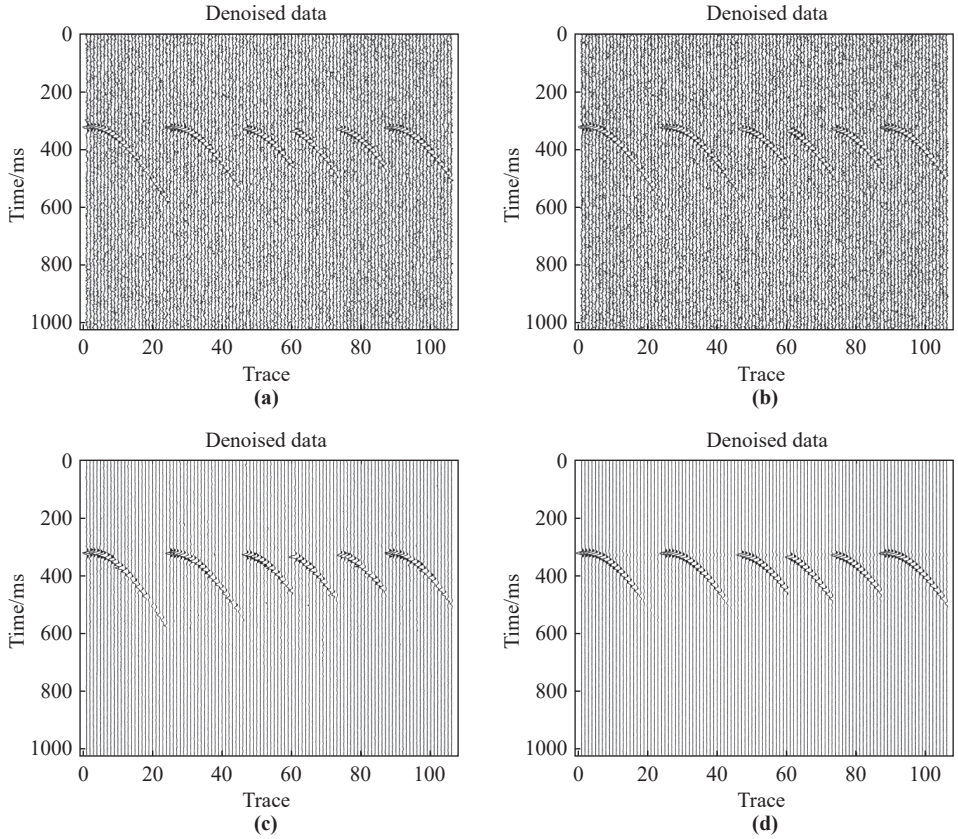

Figure 12. (a) Denoised section obtained by CEEMD. (b) Denoised section obtained by CEEMD-SVD. (c) Denoised section obtained by DAE. (d) Denoised section extracted by CEEMD-MDAE.

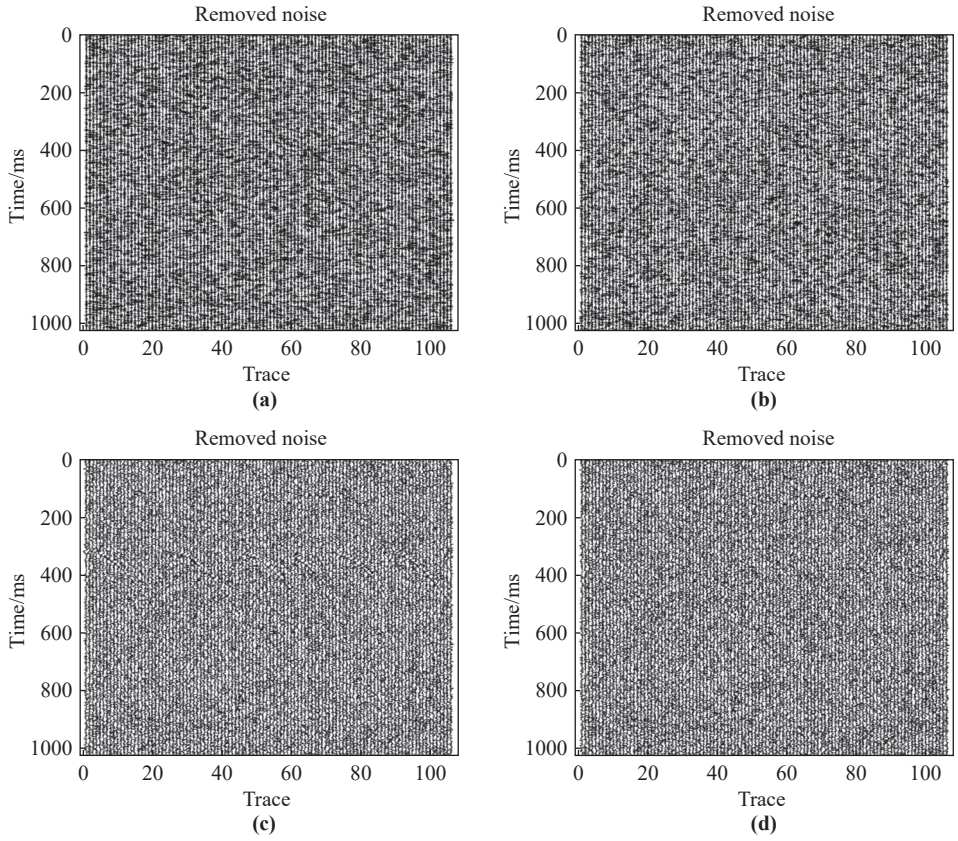

Figure 13. (a) Noise section obtained by CEEMD. (b) Noise section obtained by CEEMD-SVD. (c) Noise section obtained by DAE. (d) Noise section extracted by CEEMD-MDAE.

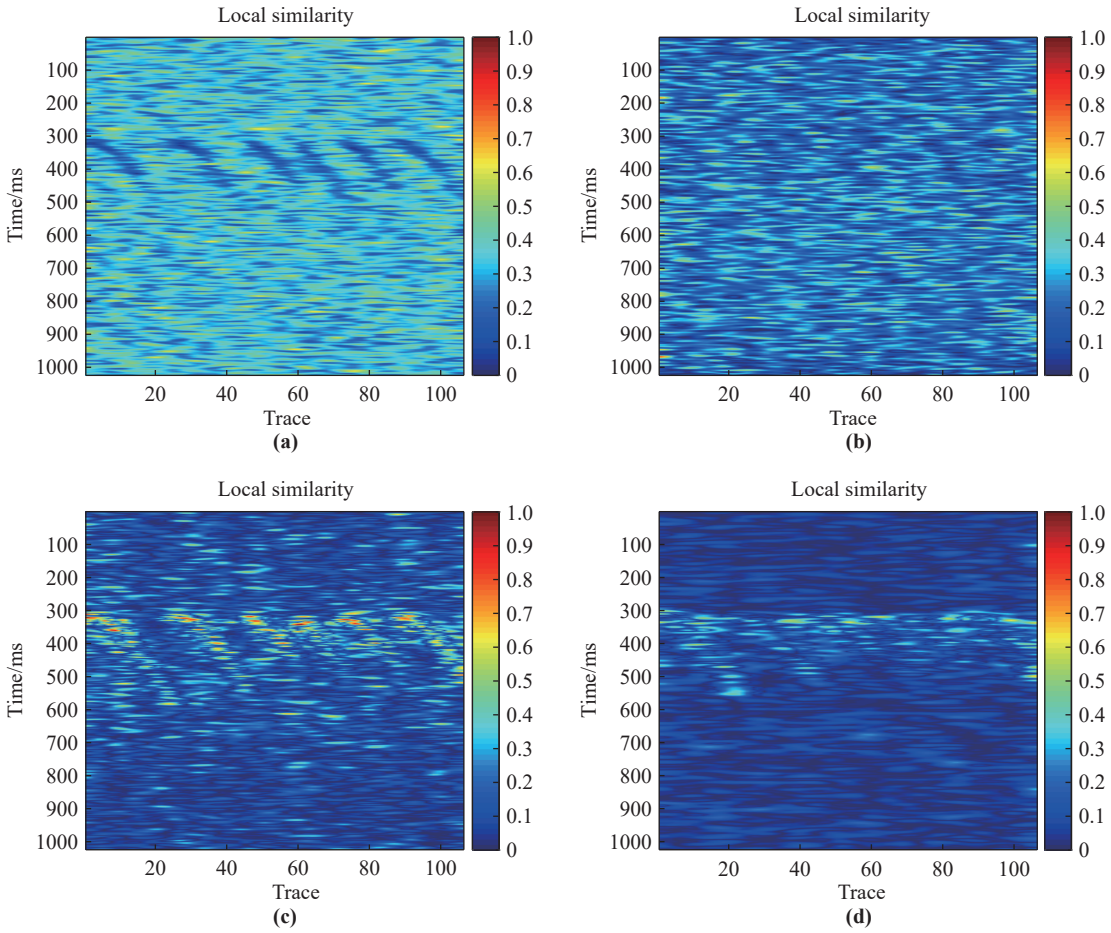

Figure 14. (a) Local similarity of the CEEMD method. (b) Local similarity of the CEEMD-SVD method. (c) Local similarity of the DAE method. (d) Local similarity of the proposed method.

In summary, the CEEMD-MDAE algorithm proposed in this paper is generally superior to other benchmark algorithms in terms of noise suppression performance for both synthetic and field data. The simulation results also demonstrate the effectiveness of the proposed algorithm in microseismic noise suppression.

5. Conclusion

In this paper, a novel CEEMD-MDAE algorithm has been proposed to attenuate noise of surface microseismic data. The CEEMD has the distinguished advantages of posteriority and adaptive decomposition. Nevertheless, the artificial identification of noise at high frequency in signals reconstruction has a passive impact on noise suppression. In order to better separate the effective signals from the noisy data, the MDAE network has been employed to extract the features of intrinsic mode function components. In the MDAE network, a novel loss function has been designed to achieve unsupervised noise attenuation in the field data. The proposed algorithm has significantly improved the SNR of the synthetic data by comparing with several benchmark algorithms. More importantly, this algorithm has better noise suppression capability and retains more weak effective signals in field surface microseismic data. It is worthwhile to mention that the developed filtering algorithm is suitable for online applications, which constitutes one of our future research topics [48–51].

Author Contributions: Chuang Guan: Conceptualization, Methodology, Software, Writing-original draft; **Lujia Zheng**: Methodology, Software, Investigation & Formal Analysis; **Chuang Wang**: Supervision, Conceptualization, Methodology, Writing-review & editing.

Funding: This work was supported in part by the National Natural Science Foundation of China under Grant 62403119, the Postdoctoral Fellowship Program of China Postdoctoral Science Foundation (CPSF) under Grant Number GZB20240136, the China Postdoctoral Foundation under Grant Number 2024MD753911, the Heilongjiang Provincial Postdoctoral Science Foundation of China under Grant Number LBH-TZ2405, and the Guiding Innovation Fund of Northeast Petroleum University(2023YDL-18).

Data Availability Statement: The data that support the findings of this study are available on request from the corresponding author upon reasonable request.

Conflicts of Interest: The authors declare no conflict of interest.

References

1. Maxwell, S.C.; Rutledge, J.; Jones, R.; *et al*. Petroleum reservoir characterization using downhole microseismic monitoring. Geophysics, **2010**, *75*: 75A129−75A137. doi: 10.1190/1.3477966
2. Sun, J.; Wang, L.G.; Hou, H.Q.. Application of micro-seismic monitoring technology in mining engineering. Int. J. Min. Sci. Technol., **2012**, *22*: 79−83. doi: 10.1016/j.ijmst.2011.06.007
3. Zhao, B.X.; Wang, Z.R.; Liu, R.; *et al*. Review of microseismic monitoring technology research. Prog. Geophys., **2014**, *29*: 1882−1888. doi: 10.6038/pg20140454(InChinese)
4. Jiang, R.C.; Dai, F.; Liu, Y.; *et al*. A novel method for automatic identification of rock fracture signals in microseismic monitoring. Measurement, **2021**, *175*: 109129. doi: 10.1016/j.measurement.2021.109129
5. Zhang, W.L.; Li, C.; Ren, J.J.; *et al*. Measurement and application of vibration signals during pressure relief hole construction using microseismic system. Measurement, **2020**, *158*: 107696. doi: 10.1016/j.measurement.2020.107696
6. Feng, Q.K.; Li, Y.. Transform learning in the synchrosqueezing frequency domain–a novel denoising strategy for optical fiber seismic records. J. Appl. Geophys., **2022**, *201*: 104648. doi: 10.1016/j.jappgeo.2022.104648
7. Zhang, C.; van der Baan, M.. Multicomponent microseismic data denoising by 3D shearlet transform. Geophysics, **2018**, *83*: A45−A51. doi: 10.1190/geo2017-0788.1
8. Mousavi, S.M.; Langston, C.A.; Horton, S.P.. Automatic microseismic denoising and onset detection using the synchrosqueezed continuous wavelet transform. Geophysics, **2016**, *81*: V341−V355. doi: 10.1190/geo2015-0598.1
9. Vera Rodriguez, I.; Bonar, D.; Sacchi, M.. Microseismic data denoising using a 3C group sparsity constrained time-frequency transform. Geophysics, **2012**, *77*: V21−V29. doi: 10.1190/geo2011-0260.1
10. Zhang, C.; van der Baan, M.. A denoising framework for microseismic and reflection seismic data based on block matching. Geophysics, **2018**, *83*: V283−V292. doi: 10.1190/geo2017-0782.1
11. Xu, Z.T.; Luo, Y.S.; Wu, B.Y.; *et al*. S2S-WTV: Seismic data noise attenuation using weighted total variation regularized self-supervised learning. IEEE Trans. Geosci. Remote Sens., **2023**, *61*: 5908315. doi: 10.1109/TGRS.2023.3268554
12. Gao, H.Y.; Zhang, M.R.; Hou, N.; *et al*. Dynamic-transmission-based recursive filtering algorithm for microseismic event detection under sensor saturations. Measurement, **2021**, *186*: 110197. doi: 10.1016/j.measurement.2021.110197
13. Han, J.J.; van der Baan, M.. Microseismic and seismic denoising via ensemble empirical mode decomposition and adaptive thresholding. Geophysics, **2015**, *80*: KS69−KS80. doi: 10.1190/geo2014-0423.1
14. Jia, R.S.; Zhao, T.B.; Sun, H.M.; *et al*. Micro-seismic signal denoising method based on empirical mode decomposition and independent component analysis. Chin. J. Geophys., **2015**, *58*: 1013−1023. doi: 10.6038/cjg20150326(InChinese)
15. Huang, N.E.; Shen, Z.; Long, S.R.; *et al*. The empirical mode decomposition and the Hilbert spectrum for nonlinear and non-stationary time series analysis. Proc. R. Soc. A Math. Phys. Eng. Sci., **1998**, *454*: 903−995. doi: 10.1098/rspa.1998.0193
16. Lin, Y.; Liao, Q.D.; Lin, Z.X.; *et al*. A novel hybrid model integrating modified ensemble empirical mode decomposition and LSTM neural network for multi-step precious metal prices prediction. Resour. Policy, **2022**, *78*: 102884. doi: 10.1016/j.resourpol.2022.102884
17. Liu, J.C.; Gu, Y.; Chou, Y.X.; *et al*. Seismic data random noise reduction using a method based on improved complementary ensemble EMD and adaptive interval threshold. Explor. Geophys., **2021**, *52*: 137−149. doi: 10.1080/08123985.2020.1777849
18. Zhao, Y.; Yue, Y.X.; Huang, J.L.; *et al*. CEEMD and wavelet transform jointed de-noising method. Prog. Geophys., **2015**, *30*: 2870−2877. doi: 10.6038/pg20150655(InChinese)
19. Sun, M.M.; Li, Z.C.; Li, Z.N.; *et al*. A noise attenuation method for weak seismic signals based on compressed sensing and CEEMD. IEEE Access, **2020**, *8*: 71951−71964. doi: 10.1109/ACCESS.2020.2982908
20. Yeh, J.R.; Shieh, J.S.; Huang, N.E.. Complementary ensemble empirical mode decomposition: A novel noise enhanced data analysis method. Adv. Adapt. Data Anal., **2010**, *2*: 135−156. doi: 10.1142/S1793536910000422
21. Zheng, H.M.; Dang, C.L.; Gu, S.M.; *et al*. A quantified self-adaptive filtering method: Effective IMFs selection based on CEEMD. Meas. Sci. Technol., **2018**, *29*: 085701. doi: 10.1088/1361-6501/aac990
22. Wang, J.W.; Zhuang, Y.; Liu, Y.S.. FSS-Net: A fast search structure for 3D point clouds in deep learning. Int. J. Network Dyn. Intell., **2023**, *2*: 100005. doi: 10.53941/IJNDI.2023.100005
23. Zhong, T.; Cheng, M.; Dong, X.T.; *et al*. Seismic random noise attenuation by applying multiscale denoising convolutional neural network. IEEE Trans. Geosci. Remote Sens., **2022**, *60*: 5905013. doi: 10.1109/TGRS.2021.3095922
24. Kasongo, S.M.. A deep learning technique for intrusion detection system using a recurrent neural networks based framework. Comput. Commun., **2023**, *199*: 113−125. doi: 10.1016/j.comcom.2022.12.010
25. Tian, Y.N.; Sui, J.L.; Li, Y.; *et al*. A novel iterative PA-MRNet: Multiple noise suppression and weak signals recovery for downhole DAS data. IEEE Trans. Geosci. Remote Sens., **2022**, *60*: 5914314. doi: 10.1109/TGRS.2022.3170635
26. Dong, X.T.; Lin, J.; Lu, S.P.; *et al*. Seismic shot gather denoising by using a supervised-deep-learning method with weak dependence on real noise data: A solution to the lack of real noise data. Surv. Geophys., **2022**, *43*: 1363−1394. doi: 10.1007/s10712-022-09702-7
27. Gao, Z.T.; Zhang, S.; Cai, J.X.; *et al*. Research on deep convolutional neural network time-frequency domain seismic signal denoising combined with residual dense blocks. Front. Earth Sci., **2021**, *9*: 681869. doi: 10.3389/FEART.2021.681869
28. Krizhevsky, A.; Sutskever, I.; Hinton, G.E. ImageNet classification with deep convolutional neural networks. In Proceedings of the 26th International Conference on Neural Information Processing Systems, Lake Tahoe, USA, 3–6 December 2012; Curran Associates Inc.: Red Hook, 2012; pp. 1097–1105.
29. Wang, T.T.; Trugman, D.; Lin, Y.Z.. SeismoGen: Seismic waveform synthesis using GAN with application to seismic data augmentation. J. Geophys. Res.: Solid Earth, **2021**, *126*: e2020JB020077. doi: 10.1029/2020JB020077
30. Wang, C.; Wang, Z.D.; Liu, Q.Y.; *et al*. Support-sample-assisted domain generalization via attacks and defenses: Concepts,

algorithms, and applications to pipeline fault diagnosis. IEEE Trans. Industr. Inform., **2024**, *20*: 6413−6423. doi: 10.1109/TII.2023.3337364

31. Zeng, N.Y.; Li, H.; Wang, Z.D.; *et al*. Deep-reinforcement-learning-based images segmentation for quantitative analysis of gold immunochromatographic strip. Neurocomputing, **2021**, *425*: 173−180. doi: 10.1016/j.neucom.2020.04.001
32. Wang, C.; Wang, Z.D.; Dong, H.L.. A novel prototype-assisted contrastive adversarial network for weak-shot learning with applications: Handling weakly labeled data. IEEE/ASME Trans. Mechatron., **2024**, *29*: 533−543. doi: 10.1109/TMECH.2023.3287070
33. Li, Z.K.; Yu, X.H.; Qiu, J.B.; *et al*. Cell division genetic algorithm for component allocation optimization in multifunctional placers. IEEE Trans. Industr. Inform., **2022**, *18*: 559−570. doi: 10.1109/TII.2021.3069459
34. Teng, J.D.. A hybrid approach of deep learning to forecast financial performance: From unsupervised to supervised. Syst. Sci. Control Eng., **2024**, *12*: 2305411. doi: 10.1080/21642583.2024.2305411
35. Gao, Y.; Zhao, P.Q.; Li, G.F.; *et al*. Seismic noise attenuation by signal reconstruction: An unsupervised machine learning approach. Geophys. Prospect., **2021**, *69*: 984−1002. doi: 10.1111/1365-2478.13070
36. Sun, Q.Q.; Liu, X.F.; Bourennane, S.; *et al*. Multiscale denoising autoencoder for improvement of target detection. Int. J. Remote Sens., **2021**, *42*: 3002−3016. doi: 10.1080/01431161.2020.1856960
37. Wang, M.Q.; Wu, Z.Y.; Sun, X.X.; *et al*. Trust-aware collaborative filtering with a denoising autoencoder. Neural Process. Lett., **2019**, *49*: 835−849. doi: 10.1007/s11063-018-9831-7
38. Li, J.H.; Struzik, Z.; Zhang, L.Q.; *et al*. Feature learning from incomplete EEG with denoising autoencoder. Neurocomputing, **2015**, *165*: 23−31. doi: 10.1016/j.neucom.2014.08.092
39. Kim, Y.; Geng, J.H.; Ney, H. Improving unsupervised word-by-word translation with language model and denoising autoencoder. In Proceedings of the 2018 Conference on Empirical Methods in Natural Language Processing, Brussels, Belgium, 31 October–4 November 2018; ACL: New York, 2018; pp. 862–868. DOI: 10.18653/v1/D18-1101
40. Saad, O.M.; Chen, Y.K.. Deep denoising autoencoder for seismic random noise attenuation. Geophysics, **2020**, *85*: V367−V376. doi: 10.1190/geo2019-0468.1
41. Wu, Z.H.; Huang, N.E.. Ensemble empirical mode decomposition: A noise-assisted data analysis method. Adv. Adapt. Data Anal., **2009**, *1*: 1−41. doi: 10.1142/S1793536909000047
42. Soulie, F.F.; Gallinari, P.; Le, Y.; Cun, Thiria, S. Automata networks and artificial intelligence. In Centre National de Recherche Scientifique *on Automata Networks in Computer Science: Theory and Applications, Paris, France, 1987*; Princeton University Press: Princeton, 1987; pp. 133–186.
43. Huang, Y.F.; Yao, Z.N.; Xu, Q.F.. Classification model of electricity consumption behavior based on sparse denoising autoencoder feature dimensionality reduction and spectral clustering. Int. J. Electr. Power Energy Syst., **2024**, *158*: 109960. doi: 10.1016/j.ijepes.2024.109960
44. Ni, L.; Liew, V.K.S.. Carbon emission price forecasting in China using a novel secondary decomposition hybrid model of CEEMD-SE-VMD-LSTM. Syst. Sci. Control Eng., **2024**, *12*: 2291409. doi: 10.1080/21642583.2023.2291409
45. Aslam, M.M.; Tufail, A.; De Silva, L.C.; *et al*. An improved autoencoder-based approach for anomaly detection in industrial control systems. Syst. Sci. Control Eng., **2024**, *12*: 2334303. doi: 10.1080/21642583.2024.2334303
46. Chen, Z.; Zhang, L.; Tang, J.M.; *et al*. Conditional generative adversarial net based feature extraction along with scalable weakly supervised clustering for facial expression classification. Int. J. Network Dyn. Intell., **2024**, *3*: 100024. doi: 10.53941/IJNDI.2024.100024
47. Li, B.W.; Li, W.L.. Distillation-based user selection for heterogeneous federated learning. Int. J. Network Dyn. Intell., **2024**, *3*: 100007. doi: 10.53941/IJNDI.2024.100007
48. Liu, Z.T.; Lin, W.Y.; Yu, X.H.; *et al*. Approximation-free robust synchronization control for dual-linear-motors-driven systems with uncertainties and disturbances. IEEE Trans. Ind. Electron., **2022**, *69*: 10500−10509. doi: 10.1109/TIE.2021.3137619
49. Gong, M.T.; Sheng, L.; Zhou, D.H.. Robust fault-tolerant stabilisation of uncertain high-order fully actuated systems with actuator faults. Int. J. Syst. Sci., **2024**, *55*: 2518−2530. doi: 10.1080/00207721.2024.2312868
50. He, X.; Wang, Y.S.; Jin, J.Y.. Bayesian inference and optimisation of stochastic dynamical networks. Int. J. Syst. Sci., **2024**, *55*: 2589−2603. doi: 10.1080/00207721.2024.2329737
51. Wang, W.; Ma, L.F.; Rui, Q.Q.; *et al*. A survey on privacy-preserving control and filtering of networked control systems. Int. J. Syst. Sci., **2024**, *55*: 2269−2288. doi: 10.1080/00207721.2024.2343734

Citation: Guan, C.; Zheng, L.; Wang, C. A Novel CEEMD-Based Multichannel Denoising Autoencoder for Noise Attenuation of Surface Microseismic Data. *International Journal of Network Dynamics and Intelligence*. 2025, 4(4), 100026. doi: 10.53941/ijndi.2025.100026